CRYSTALLIZATION KINETICS AND GIANT MAGNETO IMPEDANCE BEHAVIOR OF FeCo BASED AMORPHOUS WIRES

R.K. Roy, P. Sarkar, S. Singh, A. K. Panda, A. Mitra

National Metallurgical Laboratory (CSIR); Burma Mines; Jamshedpur, Jharkhand 831007, INDIA.

Keywords: Amorphous wire, Crystallization Kinetics, Thermal Stability, GMI Behavior

Abstract

The effects of Nb addition on crystallization kinetics and giant magneto impedance (GMI) properties of $Fe_{39}Co_{39}Si_8B_{14}$ amorphous wires prepared by in-water quenching system have been investigated. Thermal behaviors of the wires have been investigated by thermal electrical resistivity measurement and differential scanning calroimetry. The substitution of 4 at% Nb for Fe and Co increases crystallization temperature and merges two crystallization peaks into one peak, leading to a significant increase in thermal stability against crystallization for $Fe_{37}Co_{37}Nb_4Si_8B_{14}$ wire. The formation of Fe_2Nb phase due to addition of Nb increases the activation energy for crystallization from 425 to 550 kJ/mol. The GMI properties of the alloys are evaluated at driving current amplitude of 10 mA and a frequency of 400 kHz. The alloys show the single peak behavior in the GMI profile. The change in GMI properties increases from 10% at 0 at% Nb to 25% at 4 at% Nb.

Introduction

Since the discovery of the GMI effect in Co-based amorphous wires in 1994, the ferromagnetic amorphous wires are widely used in various magnetic sensors such as antitheft systems, magnetic marking and labeling, geomagnetic measurements, space research, target detection and tracking [1-3]. Due to high demand in the field engineering and industrial sectors, a large number of research works have been carried out for the improvement of GMI sensors. The main focus is on the development of new materials and subsequent processing of the materials by thermal treatment and/or tensile loading. Therefore, a thorough understanding of GMI phenomena with respect to alloy compositions and annealing temperature, time, tensile stress have a great emphasis for developing novel magnetic sensors.

The water-quenched amorphous wire preparation is dependent on three factors, i.e., (i) solidification of the metallic melt stream at high cooling rates and within the stable distance from the ejection point, (ii) use of a cooling fluid with low viscosity and surface tension, and (iii) stable and non-turbulent flow of the cooling liquid at high velocities [4]. Amongst these factors, first and second points are processing parameters and third point is dependent on alloy composition [5]. Therefore, alloy compositions should be optimized for stable and non-turbulent flow of the alloys in water, resulting in the production of defect-free and continuous wire. The optimized alloy compositions are also responsible for high GMI effect in the wires [4].

Since amorphous alloys are thermodynamically instable, the physical properties of the alloys are frequently changed with respect to both temperature and time. It hindrances amorphous alloys

used in practical applications. However, the alloys become thermodynamically equilibrium after structural relaxation and nanocrystallization at higher temperature [6]. The crystallization kinetics not only changes thermal behavior of amorphous alloys but also influences magnetic and GMI properties at different conditions [7, 8]. Moreover, the controlled crystallization causes the tailoring of the microstructure, resulting in the desired properties in nanocrystalline–amorphous matrix alloys [9, 10]. Therefore, the studies on thermal stability and crystallization kinetics of the amorphous alloys are important for its practical application. Despite several studies published in the literature about FeCo-based amorphous wires and their GMI properties, the crystallization behavior study of the wires is very little. The aim of this work is to present the effect of Nb on crystallization kinetics of the FeCoBSi based amorphous wire and subsequently the effect of structural changes on GMI properties.

Experimental Procedure

The ingots with a nominal composition of $Fe_{39}Co_{39}Si_8B_{14}$ (FC1) and $Fe_{37}Co_{37}Nb_4Si_8B_{14}$ (FC4) were prepared by arc melting the mixture of pure elements (>99.9 wt %) in an argon atmosphere. The amorphous wires of the alloys were produced by in-water quenching technique (Figure 1a). In this process, the small pieces of ingot were remelted in a quartz crucible with a nozzle diameter of 150 µm and ejected on the water of rotating drum through the nozzle under argon gas pressure of 300 kPa (Figure 1b). The amorphous wires produced from this method are 120 µm in diameter and 3-4 m in length. The structures of as-cast and annealed wires were characterized by x-ray diffractometer (XRD) using CuK_α radiation (λ= 0.1540 nm). The crystallization kinetics was investigated at different heating rates of 20, 30, 40 and 50°C/min by differential scanning calorimetry (DSC) with a Perkin-Elmer Diamond DSC under a continuous flow of purified argon. Electrical resisitivity measurement was done using thermal electrical resistivity (TER) unit of Ulvac-Riko with a heating rate of 10°C/min. The magneto-impedance was measured by the four probe technique where the driving field was generated by passing an ac current and the system was capable of generating current amplitude (I_{ac}) ranging between 1-20 mA with a maximum frequency 2000 kHz. A Helmholtz coil was used to apply a dc external magnetic field parallel to the axis of the sample. The percentage of GMI ratio ($\Delta Z/Z$) has been calculated from the first harmonic signal using the relation

$$\frac{\Delta Z}{Z}\% = \left[\frac{Z(H) - Z(H_0)}{Z(H_0)}\right] \times 100$$

where H_0= 0 kAm^{-1}, the minimum dc applied field.

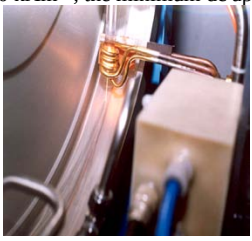

(a)

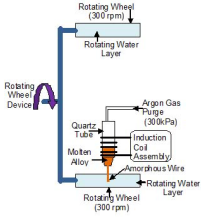

(b)

Figure 1. (a) Wire preparation by in-water quenching technique, (b) Schematic diagram of cross-sectional view of the technique.

Results and Discussion

3.1 Structure of Water Quenched Wires

Figure 2 shows the surface smoothness and structure of as-cast wire. The water-quenched as-cast represents quite smooth surface, as observed by scanning electron microscopy (SEM) image (Figure 2a). The smooth surface of the wire is dependent on the optimization of process parameters and alloy compositions. The structure of as-cast wires is basically amorphous in nature, observing by a halo diffraction peak and no appreciable crystalline peaks (Figure 2b).

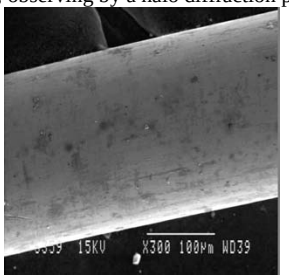

(a)

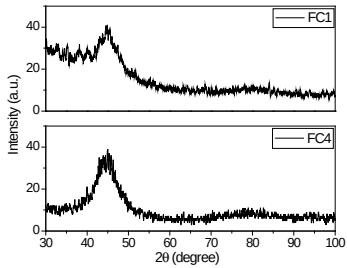

(b)

Figure 2. As-cast wires showing (a) Surface smoothness of FC1 alloy by SEM image and (b) Structure by XRD pattern

3.2 Crystallization Behavior of the Wires

The continuous scanning of the amorphous wires at the heating rate of 20°C/min is shown by DSC thermograms (Figure 3). Two peaks in FC1 and single peak in FC4 signify the multi stage and single stage crystallization of those alloys, respectively. As shown in Figure 3 and Table I, the onset and peak temperatures of FC1 are lower than that of FC4, representing higher thermal stability of FC4 alloy compared to FC1 alloy. The crystalline phases can be examined by XRD patterns of the annealed wires (Figure 4). The first and second crystallization peaks of FC1 alloy correspond to α-FeCo phase and FeB, CoB and CoSi phases, determined after annealing at 550 and 585°C, respectively. The Nb addition stabilizes α-FeCo phases and, therefore, Fe_2Nb phases are predominant and no borides and/or suicides phases are observed in FC4 alloy annealed at 630°C. The crystalline size of the phases is measured by the broadening of the X-ray diffraction patterns using Scherrer equation [11], $D= 0.9\lambda/\beta \cos\theta$, where D is crystallite size, λ is wavelength of incident radiation (0.1540 nm), β is full width at half maximum (Table II). The crystallite sizes of α-FeCo phases decrease with the effect of Nb addition. The element Nb acts as a growth inhibitor, resulting in finer nanocrystallites in the amorphous matrix [12].

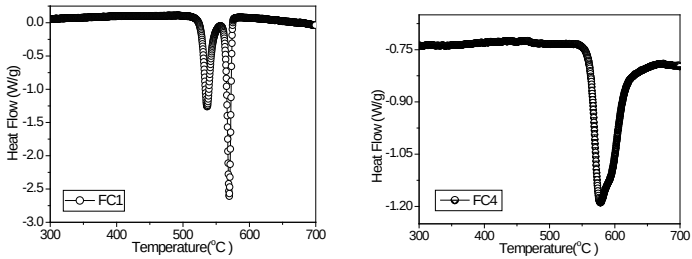

Figure 3 DSC thermograms of the amorphous wires at heating rate of 20°C/min

Table I. Onset, Peak, End Temperatures and Activation Energy for Crystallization of FC1& FC4 Wires

Alloy Name	**Onset Temp.(°C)**	**Peak Temp.(°C)**	**End Temp.(°C)**	**Activation Energy (Ea), kJ/mol**
FC1, First Peak	527	535	545	278
FC1, Second Peak	564	570	574	388
FC4	563	578	620	458

Table II. Crystallite Sizes (nm) of Various Phases Formed in FC1, FC4 Alloys after Annealing

Alloy name & Annealing Temperature	**Fe-Co Phase (nm)**	**Fe_2Nb Phase (nm)**
FC1 & ann. at 550°C	21.1	-
FC1 & ann. at 585°C	23.4	-
FC4 & ann. at 575°C	16.3	13.3
FC4 & ann. at 630°C	17.0	13.4

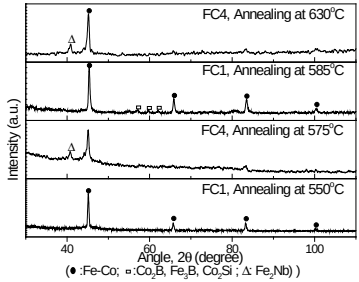

Figure 4. XRD patterns of annealed wires

The apparent activation energy of crystallization (E_a) for each observed crystallization step can be determined by Kissinger's relationship between the exothermic peak temperature (T_p) and the heating rate (h) [13], described as the equation (1)

$$\ln \frac{h}{T_p^{\,2}} = -\frac{E_a}{RT_p} + \text{constant} \qquad (1)$$

where R is a gas constant.

According to equation (1), the plotting of $\ln(h/T_p^{\,2})$ as a function of $1/T_p$ yields a straight line and activation energy (E_a) is determined from the slope ($-E_a/R$) of the lines (Table I). The activation energy of solid state reactions is spent for overcoming and lowering of the activation barrier due to rearrangements of atoms [14]. It results in the formation of nuclei and their growth during crystallization. Therefore, the energy calculated in these experiments, is determined for both the lowering of the potential activation barrier and overcoming the barrier. The activation energy of crystallization increases during addition of Nb, indicating the role of a significant fraction of the atoms in the structural reorganization. It causes the formation of stable Fe_2Nb phase in FC4 alloy, and improves the thermal stability of the alloy.

3.3 Electron Transport Properties of Wires during Annealing

The order-disorder change and nanocrystallization behaviour in amorphous alloys can be evaluated by electrical resistivity measurement. Figure 5 represents the variation of normalized resistivity of amorphous wires during isochronal annealing at the heating rate of 10°C/min. In all the alloys, the resistivity initially increases with temperature and then suddenly drops at the T_{x1}. It is attributed to the transformation of largely disordered metastable amorphous state to the ordered crystalline state [15]. Therefore, T_{x1} is the first crystallization temperature. The T_{x1} shifts to higher temperature with the addition of Nb in FC4 alloy. The second crystallization (T_{x2}) also occurs at higher temperatures for FC4 alloy than FC1 alloy. After the completion of second crystallization, the growing nanophase particles lead to grain boundary scattering and consequent increase in resistivity.

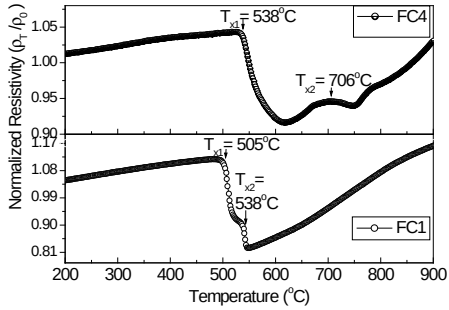

Fig. 5 Electrical resistivity measurements of amorphous wires at the heating rate of 10°C/min

3.4 Variation of Magnetic Moments with Temperature

The thermal variation of magnetic moments of the as-cast wires was measured to study the effect of crystallization process on Curie temperature (Figure 6). The initial sharp drop is associated with the curie temperature of the amorphous matrix. The curie temperature is highest in FC1 alloy and decreases with the addition of Nb in other alloy. At T_c, the sudden drop of magnetic moments in FC1 and FC4 may be attributed to the rapid transition of ferro-to-para magnetism, however, the continuous reduction of magnetic moments in FC4 alloy is due to sluggish transition from ferromagnetism to paramagnetism. The magnetic moment of FC1 alloy suddenly reverts back to initial stage, indicating ferromagnetic coupling is largely present in that alloy and it is rapidly changing its mode.

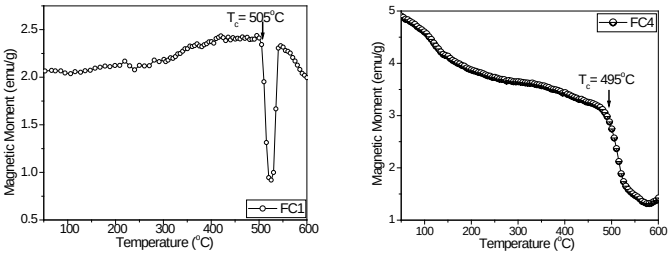

Figure 6. Change of magnetic moments as a function of temperature

3.5 GMI Properties of the Alloys

The composition dependence of GMI ratio is explained for the as-received alloys in Figure 7. The curves show the single-peak GMI characteristics behaviour and are sharpen with the addition of Nb in the master alloy of $Fe_{39}Co_{39}Si_8B_{14}$ (FC1) for FC4 alloy. The improvement of GMI properties is due to the change in skin depth of the wire after addition of Nb [7, 16]. The skin effect of amorphous wire is also dependent on ac frequency and amplitude of ac driving field. Initially, the GMI ratio increases and then it decreases above 400 kHz frequency (Figure 8a). The dependency of amplitude of driving field on GMI effect also follows similar trend. The maximum GMI ratio is observed at 10mA driving field (Figure 8b). The GMI response is at highest when frequency and driving field are in the range of 300 kHz $\leq f \leq$ 500 kHz and $8 \leq I_{ac} \leq$ 12, respectively. It is noted that the addition of Nb is more effective to enhance magnetic impedance in all ranges of frequency and ac driving field. On the other hand, the skin depth is determined by the circular permeability that is strongly frequency dependent [16]. It causes the rise of GMI ratio to maximum range and follows a decrease with an increasing frequency within the range from 100 kHz to 10MHz. Therefore, the enhanced GMI effect is a direct consequence of the higher mobility of domain walls as correlated with transverse permeability and transverse magnetic anisotropy which are induced on the wire's surface during the rapid quenching of wire in the water [17].

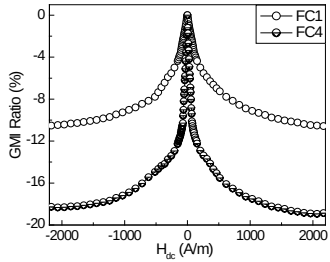

Figure 7. GMI ratio of amorphous wires at frequency of 400 kHz and field amplitude of 10mA

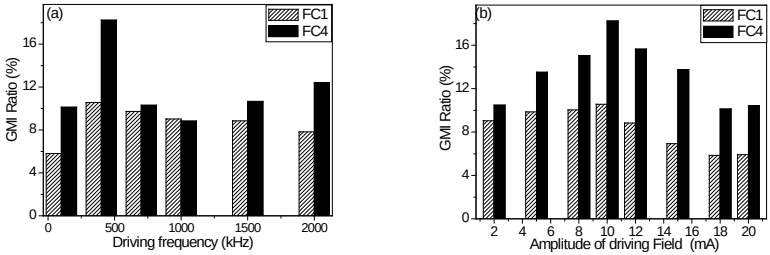

Figure 8. GMI Ratio of different wires as a function of (a) frequency at the driving field of amplitude 10mA and (b) amplitude of driving field at frequency of 400 kHz.

Conclusions

It is concluded that crystallization kinetics and GMI properties of amorphous wires are greatly changed with the addition of Nb in the master alloy of $Fe_{39}Co_{39}Si_8B_{14}$ as follows:

1) Crystallization of FC1 alloy takes place in two stages, while FC4 follows single stage crystallization.
2) Thermal stability and activation energy of crystallization increases in FC4 alloy due to the formation of stable phases like Fe_2Nb.
3) The Nb addition does not affect much in curie temperature of FC4 alloy than that of FC1 alloy.
4) The GMI ratio is 18% for FC4 alloy and 10% for FC1 alloy.
5) The GMI response of all alloys is at the highest when frequency and driving field are in the range of 300 kHz $\leq f \leq$ 500 kHz and $8 \leq I_{ac} \leq 12$, respectively.

Acknowledgement

We express our thanks to the Director, National Metallurgical Laboratory (CSIR), Jamshedpur, for giving us permission to publish the work. The work is a part of the CSIR network project on “Nanostructured Advanced Materials” (NWP-051).

References

1. L.V. Panina, K. Mohri, "Giant magnetic field dependent impedance of amorphous FeCoSiB wire", *Appl Phys Lett*, 65 (1994), 1189–91.
2. T. Meydan, *J Magn Magn Mater*, "Application of amorphous materials to sensors", 133 (1995), 525–32.
3. J.E. Lenz, "A Review of Magnetic Sensors", *Proc. IEEE*, 78 (1990), 973–89.
4. M. H. Phan, H. X. Peng, "Giant magnetoimpedance materials-Fundamentals and applications"' *Prog. in Mat. Sc.*, 53 (2008), 323–420.
5. A.O. Olofinjana, J.H. Kern, H.A. Davies, "Effects of process variables on the multi-strand casting of high strength sub-millimetre metallic glass wire", *J. Mater. Proc. Tech.*, 155–156 (2004), 1344–1349.
6. Z. Stokłosa, J. Rasek, P. Kwapuliński, G. Haneczok, G.Bzdura, J. Lelątko, "Nanocrystallisation of amorphous alloys based on iron", *Mat. Sc. and Engg C*, 23 (2003), 49 – 53.
7. D. Y. Liu, W.S. Sun, H.F. Zhang, Z.Q. Hu," Preparation, thermal stability and magnetic properties of Fe–Co–Ni–Zr–Mo–B bulk metallic glass" *Intermetallics*, 12 (2004), 1149–1152.
8. W.S. Sun, T. Kulik, X.B. Liang, J. Ferenc, "Thermal stability and magnetic properties of Co–Fe–Hf–Ti–Mo–B bulk metallic glass", *Intermetallics*, 14 (2006), 1066–1068.
9. S. Li, S. Bai, H. Zhang, K. Chen, J. Xiao, "Effects of Nb and C additions on the crystallization behavior, microstructure and magnetic properties of B-rich nanocrystalline Nd–Fe–B ribbons", *J. Alloys Compd*., 470 (2009), 141.
10. S.W. Du, R.V. Ramanujan, "Crystallization and magnetic properties of Fe40Ni38B18Mo4 amorphous alloy", *J. Non-Cryst. Solids*, 351 (2005), 3105.
11. M.P. Klug, L.F. Alexanader, *X-ray Diffraction Procedures for Polycrystalline and Amorphous Materials*, (John Wiley & Sons, New York, 1974) 634.
12. K. J. Miller, A. Leary, S. J. Kernion, A. Wise, D. E. Laughlin, M. E. McHenry, Vladimir Keylin, and Joe Huth," Increased induction in FeCo-based nanocomposite materials with reduced early transition metal growth inhibitors", *J. of App. Phy*, 107 (2010) 09A316.
13. H. E. Kissinger, "Reaction Kinetics in Differential Thermal Analysis", *Anal. Chem*., 29 (1957), 1702.
14. D. .M. Minić, A. Gavrilović, P. Angerer, D.G. Minić, A. Maričić," Thermal stability and crystallization of $Fe_{89.8}Ni_{1.5}Si_{5.2}B_3C_{0.5}$ amorphous alloy", *J. of Alloys and Comp.*, 482 (2009), 502–507.
15. W. Teoh, N. Teoh, S. Arajs, *Amorphous Magnetism II*, (R. Levy, R. Hasegawa (Eds.), Plenum Press, New York, 1977) 327.
16. M. Vazquez, *J. of Mag. and Magn. Mater*., "Giant magneto-impedance in soft magnetic "Wires"", 226-230 (2001), 693-699.
17. N.D. Tho, N. Chau, S.C. Yu, H.B. Lee, N.D. The, N.Q. Hoa, "A systematic study of giant magnetoimpedance of Cr-substituted $Fe_{(73.5-x)}Cr_xSi_{13.5}B_9Nb_3Au_1$ (x=1, 2, 3, 4, 5) alloys", *J. of Magn. and Magn. Mater*., 304 (2006), e871–e873